

Thermal Entropy, Density Disorder and Antiferromagnetism of Repulsive Fermions in 3D Optical Lattice

Yu-Feng Song,^{1,2} Youjin Deng,^{1,3,*} and Yuan-Yao He^{2,4,3,†}

¹Hefei National Laboratory for Physical Sciences at Microscale and Department of Modern Physics, University of Science and Technology of China, Hefei, Anhui 230026, China

²Institute of Modern Physics, Northwest University, Xi'an 710127, China

³Hefei National Laboratory, University of Science and Technology of China, Hefei 230088, China

⁴Shaanxi Key Laboratory for Theoretical Physics Frontiers, Xi'an 710127, China

(Dated: November 21, 2024)

The celebrated antiferromagnetic phase transition was realized in a most recent optical lattice experiment for 3D fermionic Hubbard model [Shao *et al.*, Nature **632**, 267 (2024)]. Despite the great achievement, it was observed that the AFM structure factor (and also the critical entropy) reaches the maximum around the interaction strength $U/t \simeq 11.75$, which is significantly larger than the theoretical prediction as $U/t \simeq 8$. Here we resolve this discrepancy by studying the interplay between the thermal entropy, density disorder and antiferromagnetism of half-filled 3D Hubbard model with numerically exact auxiliary-field quantum Monte Carlo simulations. We have achieved accurate entropy phase diagram, which allows us to simulate arbitrary entropy path on the temperature-interaction plane and to track the experimental parameters. We then find that above discrepancy can be quantitatively explained by the *entropy increase* as enhancing the interaction in experiment, and together by the lattice *density disorder* existing in the experimental setup. We furthermore investigate the entropy dependence of double occupancy, and predict its universal behaviors which can be used as useful probes in future optical lattice experiments.

Quantum simulation combining ultracold atoms and optical lattice potentials [1, 2] has become an essential route to study the intriguing phenomena of strongly correlated systems. One representative is the fermionic Hubbard model [3–5], for which the optical lattice experiment, equipped with modern cooling, trapping and precision measurement techniques [6–8], allows for exploring broader parameter regimes than those accessible in real materials, such as tuning the interaction strength. Since the early stage, the theoretical interests on Hubbard model [9, 10] range from quantum magnetism [11–13] to fermionic superfluidity [14–16] and more subtle d -wave superconductivity [17, 18], which are also the center pursuits of the optical lattice experiment nowadays. Especially in the past decade, the experimental studies of the antiferromagnetic (AFM) spin correlation in repulsive Hubbard model [19–25] has stood in line with or even surpassed the most advanced precision many-body computations [10].

An inspiring progress on this aspect is the observation of AFM phase transition (Néel transition) in 3D Hubbard model with ultracold fermionic ${}^6\text{Li}$ atoms in a large-scale and nearly uniform optical lattice ($\sim 800,000$ sites) [25], which has attracted widespread attention [26, 27]. The transition from paramagnetic (PM) to Néel AFM ordered phase was revealed via the critical scaling of the measured AFM structure factor with the critical exponent from the Heisenberg universality class [28]. However, several significant issues still exist in the interpretation for this experiment as well as its comparison with the theory. First, the experimental measurements followed irregular paths on the temperature-interaction (T -

U) plane characterized the entropy instead of temperature [25]. This complicates the direct comparisons with previous many-body numerical calculations of 3D Hubbard model [29–44], which typically presented results as a function of T or U . Second, at half filling, the maximum of the AFM structure factor and the critical entropy appears around $U/t \simeq 11.75$ in the experiment, in contrast to $U/t \simeq 8$ from the fixed-temperature calculations with unbiased auxiliary-field quantum Monte Carlo (AFQMC) [35]. To correctly understand this disagreement and its underlying physics is crucial for the next-step and quantitative studies of the metal-insulator crossover (MIC) in PM phase [34] and more abundant phenomena with doping [41, 43] of 3D Hubbard model in the experiment. The other quantifiable issue in the experiment is the lattice density disorder inherited from the creation of the box trap potential [25]. Its effect on various properties of the model, especially the AFM spin correlation, remains to be explored.

In this work, we aim at bridging the gap between the experiment and theory, and resolve the above discrepancy, via performing numerically exact AFQMC calculations for half-filled 3D Hubbard model in a manner closely related to the experiment. In particular, we take thermal entropy as the central metric, and establish the full map of the entropy per particle (s) on the T - U plane. To mimic the experimental measurements, we compute the AFM structure factor (S_{AFM}^{zz}) along representative entropy paths, and observe that the *entropy increase* (not the trivial heating effect) can induce the peak location shifting of S_{AFM}^{zz} towards larger U . We find that this phenomenon can be also contributed by the *density*

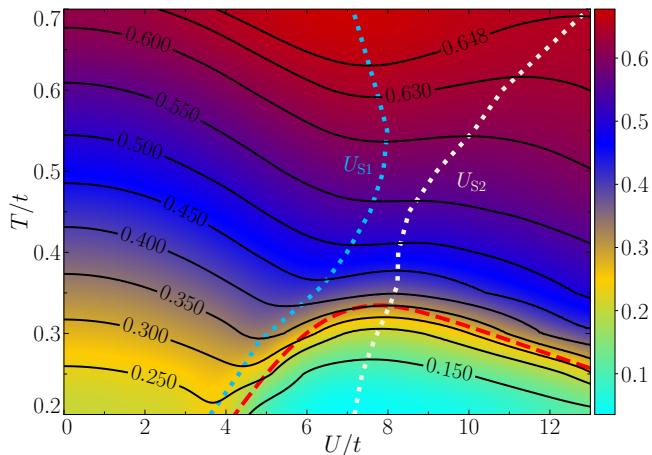


FIG. 1. Entropy phase diagram of repulsive 3D Hubbard model at half filling from our AFQMC calculations. Black solid lines are the isentropic curves with the \mathbf{s} values (in units of k_B) marked on the lines. The residual finite-size effect is negligible. The Néel temperatures (T_N , red dashed line), and the positions of local maximum (U_{S1} , light blue dashed line) and local minimum (U_{S2} , white dashed line) of \mathbf{s} at fixed temperatures from Ref. 35 are also included.

disorder. We also investigate the universal behaviors of double occupancy versus \mathbf{s} when cooling the system.

The Hubbard Hamiltonian is $\hat{\mathcal{H}} = \sum_{\mathbf{k}\sigma} \varepsilon_{\mathbf{k}} c_{\mathbf{k}\sigma}^+ c_{\mathbf{k}\sigma} + U \sum_{\mathbf{i}\sigma} [\hat{n}_{\mathbf{i}\uparrow} \hat{n}_{\mathbf{i}\downarrow} - (\hat{n}_{\mathbf{i}\uparrow} + \hat{n}_{\mathbf{i}\downarrow})/2] + \mu \sum_{\mathbf{i}\sigma} (\hat{n}_{\mathbf{i}\uparrow} + \hat{n}_{\mathbf{i}\downarrow})$, where $\hat{n}_{\mathbf{i}\sigma}$ is the density operator with \mathbf{i} labeling a site of the 3D optical lattice and $\sigma = \uparrow, \downarrow$ denoting the two hyperfine states of the ultracold atoms. The kinetic energy dispersion reads $\varepsilon_{\mathbf{k}} = -2t \sum_{\alpha=x,y,z} \cos k_{\alpha}$ with the nearest-neighbor hopping t and the momentum k_{α} defined in units of $2\pi/L$ (the lattice size is $N_s = L^3$). We set t as energy unit, and focus on the model with repulsive interaction $U > 0$ and at half filling ($\mu = 0$). Both the algorithmic and simulation details of the AFQMC calculations can be referred in our previous work [34, 35], in which we compute the Néel temperatures and explore the MIC physics in PM phase of half-filled 3D Hubbard model from a purely theoretical aspect. In this work, we take a step further to enable our numerical simulations to shake hands with the experiment.

It is the thermal entropy \mathbf{s} instead of temperature which is directly controlled and measured in optical lattice experiments. In numerics, we first compute \mathbf{s} versus U for an ensemble of fixed temperatures (with sufficiently small interval) [35], and then we perform an interpolation for the numerical data to achieve the full map of \mathbf{s} on the T - U plane as presented in Fig. 1. Our results are surely more compact and reliable than the previously reported isentropic properties for half-filled 3D Hubbard model [37, 38], which applied numerical methods with uncontrolled approximations. As expected, the AFM phase (below the T_N line as Néel transition) has the globally small entropy due to AFM long-range order. In compari-

son, \mathbf{s} in PM phase exhibits significantly more abundant structures which is closely related to the MIC [34, 35] and effective Heisenberg physics.

The most prominent feature of the entropy map in Fig. 1 is the non-monotonic behavior of the isentropic curves $T_i(U)$, along which $\mathbf{s}(T_i(U), U) = \mathbf{s}_i$ as a constant. With enhancing U , The isentropic temperature $T_i(U)$ first decreases, then increases in the middle, and finally decays again. This feature can be understood from the fixed-temperature behavior of \mathbf{s} versus U as follows. The total derivative of $\mathbf{s}(T_i(U), U) = \mathbf{s}_i$ as $d\mathbf{s} = (\partial\mathbf{s}/\partial T)dT + (\partial\mathbf{s}/\partial U)dU = 0$ yields

$$\left. \frac{\partial\mathbf{s}}{\partial U} \right|_{T=T_i} = -\frac{c(T_i)}{T_i} \frac{dT_i(U)}{dU}, \quad (1)$$

with $c(T) = T \times (\partial\mathbf{s}/\partial T)$ denoting the specific heat which is positive for $T > 0$. This equality clearly shows that the slope sign of $T_i(U)$ is opposite to that of $\mathbf{s}(T, U)$ versus U at $T = T_i$, and their extreme points as $dT_i/dU = 0$ and $(\partial\mathbf{s}/\partial U)|_{T=T_i} = 0$ should coincide at the same U value. It was previously shown [35] that, $\mathbf{s}(T, U)$ at fixed T first increases in Fermi liquid regime and reaches a local maximum (U_{S1} in Fig. 1), and then decreases as entering the MIC regime and develops a local minimum (U_{S2} in Fig. 1), and finally increases to $\ln(2)$. This corresponds to $+$, $-$, $+$ as the signs of $(\partial\mathbf{s}/\partial U)|_{T=T_i}$ in the three regimes separated by U_{S1} and U_{S2} , which renders $-$, $+$, $-$ signs of dT_i/dU respectively according to Eq. (1), and thus explains the shape of $T_i(U)$ curves. We also observe that the extreme points of $T_i(U)$ are well consistent with U_{S1} and U_{S2} curves, which furtherly confirms the above discussion.

Remarkably, the interaction-induced adiabatic cooling exists in both $U < U_{S1}$ and $U > U_{S2}$ regimes, as the decreasing $T_i(U)$ versus increasing U along the isentropic curves. Nevertheless, this effect was only revealed for the weakly interacting regime (corresponding to $U < U_{S1}$ in our work) of Hubbard models in previous studies [37, 38, 45]. For $U > U_{S2}$, the isentropic curves should possess the asymptotic behavior of $T_i(U) \propto 1/U$ towards $U \rightarrow \infty$, as approaching $T_i(U)/J = \alpha$ at which the effective AFM Heisenberg model with the coupling $J = 4t^2/U$ has the same entropy. Consequently, the T_N line should finally merge to the isentropic curve with $\mathbf{s}_i = 0.341k_B$ as the critical entropy of 3D AFM Heisenberg model [46], which is again confirmed in Fig. 1.

With the above entropy results, we can then take arbitrary entropy path to compute the AFM structure factor defined as $S_{\text{AFM}}^{zz} = N_s^{-1} \sum_{\mathbf{ij}} (-1)^{i+j} (\langle \hat{s}_{\mathbf{i}}^z \hat{s}_{\mathbf{j}}^z \rangle - \langle \hat{s}_{\mathbf{i}}^z \rangle \langle \hat{s}_{\mathbf{j}}^z \rangle)$ with $\hat{s}_{\mathbf{i}}^z = (\hat{n}_{\mathbf{i}\uparrow} - \hat{n}_{\mathbf{i}\downarrow})/2$. (Note a factor $4\times$ difference in the definition with that used in Ref. 25.) The experiment measured S_{AFM}^{zz} versus U along some unknown path crossing the AFM phase on T - U plane, and observed a S_{AFM}^{zz} peak at $U_{\text{peak}} \simeq 11.75t$. However, previous AFQMC results from fixed- T calculations [35] showed that $U_{\text{peak}} \simeq 8t$ around the highest $T_N^{\text{max}} = 0.334t$ and it

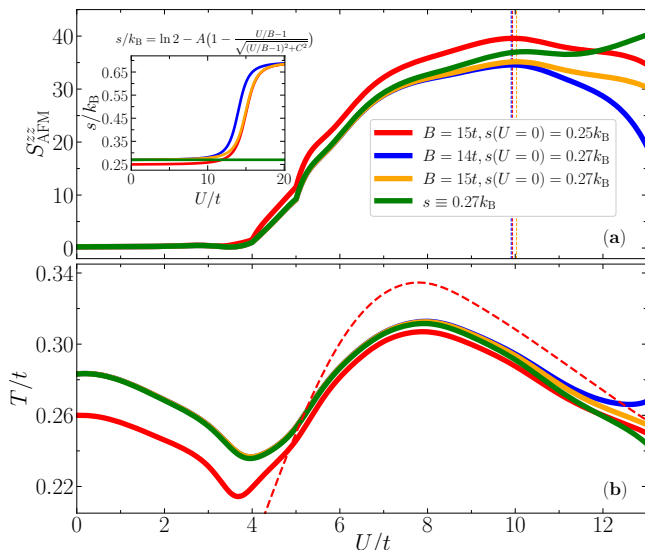


FIG. 2. Numerical results of (a) AFM structure factor S_{AFM}^{zz} and (b) the temperatures T/t as a function of U/t , along representative entropy paths. Beside the isentropic path with $s \equiv 0.27k_B$ (green solid line), the other three paths (red, blue and yellow solid lines) follow the relation $s/k_B = \ln(2) - A[1 - (U/B - 1)/\sqrt{(U/B - 1)^2 + C^2}]$ with three different sets of A, B, C parameters, and are plotted in the inset of (a). The B parameter and the initial entropy $s(U=0)$ for the paths are illustrated in the legend. The vertical dashed lines in panel (a) mark the S_{AFM}^{zz} peak locations, and the Néel temperatures T_N (red dashed line) is included in panel (b).

only slightly moves to a larger value ($< 8.6t$) in the temperature range $0.25 \leq T/t \leq 0.40$. To understand this disagreement, we first build the S_{AFM}^{zz} map [47] on T - U plane adopting similar interpolation scheme for AFQMC results at various temperatures, which consists of $L = 12$ data for $T/t \leq 0.35$ and converged results (to thermodynamic limit) for $T/t \geq 0.40$.

Then combining the maps of s and S_{AFM}^{zz} , we can design specific entropy paths resembling the experiment, and directly read out the corresponding results of S_{AFM}^{zz} . This allows us to go beyond the typical scopes of fixed- T or fixed- U calculations. First of all, a special choice is along the isentropic curve meaning adiabatically increasing U . As shown in Fig. 2(a), for $s(T_i(U), U) \equiv 0.27k_B$ as the critical entropy for $U/t = 11.75$ (in the sense of initial single-particle entropy at $U=0$) obtained in the experiment [25], S_{AFM}^{zz} is firstly small in Fermi liquid regime, then has a rapid enhancement across the Néel transition, and finally grows smoothly to the large U limit. Thus, S_{AFM}^{zz} does not even develop a peak versus U , as the isentropic curve stays inside the AFM phase [see Fig. 2(b)] once entering it and S_{AFM}^{zz} should monotonically increase and converge to the Heisenberg result. This is qualitatively different from the experimental results, and thus confirms the non-adiabatic nature of measurements with increasing U . We then

choose the specially designed entropy paths depicted by $s/k_B = \ln(2) - A[1 - (U/B - 1)/\sqrt{(U/B - 1)^2 + C^2}]$. In this formula, $s/k_B = \ln 2$ is guaranteed as the entropy at $U/t = \infty$ (only contributed by the spin degree of freedom), and the initial entropy $s(U=0)$ can be tuned by (A, B, C) parameters with $U = B$ as the fastest increasing location. Considering that S_{AFM}^{zz} almost vanishes at $U/t \simeq 20$ (and thus s/k_B should be close to $\ln 2$) and the critical entropy $s_N = 0.27k_B$ for $U/t = 11.75$ [25], we adopt three sets of parameters, one as $B = 15t$ and $s(U=0) = 0.25k_B$, and the other two as $B = 14t$ and $B = 15t$ with the same $s(U=0) = 0.27k_B$. As plotted in the inset of Fig. 2(a), these entropy paths also account for the experimental feature as nearly adiabatic evolution for small U and severely non-adiabatic process for $U/t > 10$. The numerical results of S_{AFM}^{zz} and the temperature curves corresponding to these paths are presented in Fig. 2. We can observe that peaks in S_{AFM}^{zz} clearly appear around $U/t \simeq 10$ [see Fig. 2(a)], which is indeed closer to the experimental observation comparing to fixed- T numerical result of $U_{\text{peak}}/t \simeq 8$. Moreover, the curve structure and the peak location of S_{AFM}^{zz} depends on B and $s(U=0)$ of the path. The formation of the peak can be attributed to the suppression of S_{AFM}^{zz} due to the re-entrance into PM phase with $U/t > 12$ [see Fig. 2(b)]. We have also tested entropy paths with similar features but described by rather different formulas, and find that the peak properties of S_{AFM}^{zz} and the $\Delta U_{\text{peak}} \sim 2t$ shifting as discussed above still exists. Besides, we know that, theoretically, S_{AFM}^{zz} diverges inside AFM phase and converges to a finite value in PM phase. As a result, the S_{AFM}^{zz} peak should become sharper in a large-scale system, as found in experimental results. We emphasize that the *entropy increase* encoded in above entropy paths is different from the trivial heating effect, as the actual temperatures for the paths [see Fig. 2(b)] can decrease versus U in the regions of $U/t \leq 4$ and $8 \leq U/t \leq 12$. These numerical results clearly demonstrate that *entropy increase* in experimental measurements with increasing U can indeed induce the S_{AFM}^{zz} peak at a larger U value comparing to the fixed- T numerical result.

We then turn to the lattice *density disorder* effect on the AFM structure factor of the model. In AFQMC calculations, we implement a Gaussian disorder by adding a site-dependent chemical potential term $+\sum_i \mu_i (\hat{n}_{i\uparrow} + \hat{n}_{i\downarrow})$ to the Hamiltonian, with μ_i generated by sampling with the normal distribution $P(\mu_i) = e^{-\mu_i^2/2}/\sqrt{2\pi}$ with $\bar{\mu} = 0$ and $\sigma_\mu = t$ as the average and standard deviation. Such calculations guarantee the overall half-filling condition, and also render the normal distribution feature for the lattice density results. Thus, it should be more reasonable and fits better to the experiment [25], than the uniform disorder adopted in a previous study [31]. For every set of parameters, we find that ~ 10 disorder realizations are sufficient to reach the converged disorder average results of AFM spin correlations and S_{AFM}^{zz} . The simula-

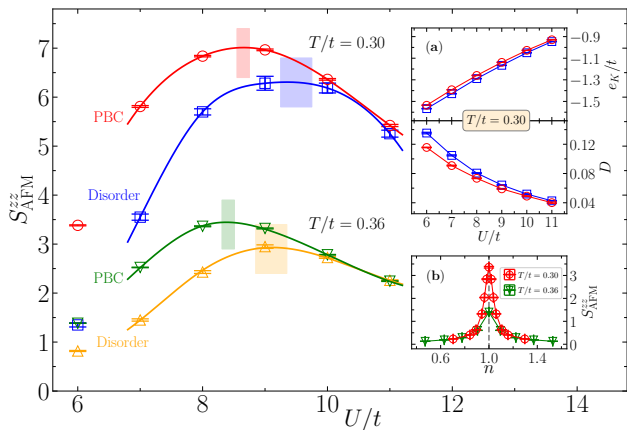


FIG. 3. Comparisons of AFM structure factor S_{AFM}^{zz} results versus U/t within periodic boundary conditions (“PBC”, without disorder) and lattice *density disorder* (“Disorder”) for $T/t = 0.30$ and $T/t = 0.36$. The vertical shading bands denote the peak locations of S_{AFM}^{zz} . The inset (a) plots the comparisons of kinetic energy per site e_K/t and double occupancy D between “PBC” and “Disorder” calculations for $T/t = 0.30$. The inset (b) presents the S_{AFM}^{zz} results from “PBC” versus the fermion filling. These results are from $L = 6$ system.

tion with above disorder is unfortunately limited to $L = 6$ system due to fermion sign problem.

In Fig. 3, we present the comparisons of S_{AFM}^{zz} versus U/t from AFQMC calculations with (“Disorder”) and without (“PBC”) *density disorder* at $T/t = 0.30$ and 0.36 . We can observe that the S_{AFM}^{zz} peak possesses a $\Delta U_{\text{peak}} \sim t$ shifting, which tends to be larger at lower temperature. This shifting can be understood from the fact that, the disorder typically suppresses the correlation length of AFM spin correlation, and thus reduces the S_{AFM}^{zz} result, which is generally more prominent in the small to intermediate U regimes. With strong interaction, the system evolves into a Mott insulator state [35] which is almost immune to the disorder effect (given μ_i is smaller than the gap). As a result, a stronger *density disorder* can produce a larger shifting of U_{peak} . Moreover, the lower kinetic energy and more double occupancy with disorder [inset (a) of Fig. 3] also reveal that the disordered system is more itinerant than the uniform system. These results together suggests that the *density disorder* effectively weakens the interaction of the system. Thus, it is important to consider this issue in the benchmark between experiment and theory. The *density disorder* should also be responsible for the relatively small S_{AFM}^{zz} results as measured in Ref. 25 especially at low temperatures, comparing to results of perfectly uniform system. For example, the finite-size scaling analysis [35] yielded the relation $S_{\text{AFM}}^{zz} L^{\eta-2} \simeq 0.2$ (with $\eta = 0.0375$) at Néel transition for $U/t = 10$. This predicts $S_{\text{AFM}}^{zz} \simeq 1454$ for the uniform system with the same size as that in experiment, comparing to the maximal $S_{\text{AFM}}^{zz} \simeq 30$ measured

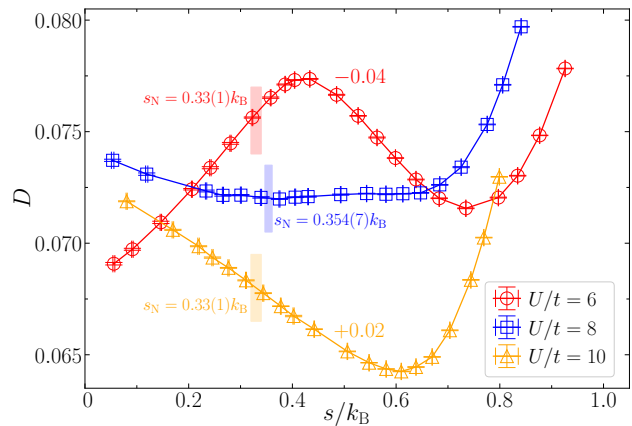


FIG. 4. Double occupancy D as a function of the entropy per particle s for $U/t = 6, 8$ and 10 . For $U/t = 6$ and $U/t = 10$, the results are shifted by -0.04 and $+0.02$ for the plot. The corresponding critical entropy values with uncertainties are marked by the vertical shading bands. The residual finite-size effect is negligible.

for $U/t = 11.75$ inside AFM phase. (We learned from our experimental colleagues in Ref. 25 that, with further improvement of the experimental system, the maximum of S_{AFM}^{zz} been significantly enhanced up to 150 [48].) This significant suppression of S_{AFM}^{zz} can be understood from the quantitative equivalence between adding the disorder and locally doping the uniform system. For the latter, S_{AFM}^{zz} rapidly decays away from half filling within $L = 6$ [inset (b) of Fig. 3], which should be even more significant with increasing L .

Computing physical observables as a function of the entropy s instead of temperature is crucial for the benchmark with optical lattice experiment [25, 39]. Here we report AFQMC results of the double occupancy $D = N_s^{-1} \sum_i \langle \hat{n}_{i\uparrow} \hat{n}_{i\downarrow} \rangle$ versus s , as presented in Fig. 4. All the curves $D(s)$ should start from the special point ($D = 1/4, s/k_B = 2 \ln 2$) as the high- T limit. Upon cooling, we can observe quite different behaviors as well as some universal signatures in $D(s)$ for $U/t = 6, 8, 10$, as representatives of weak, intermediate and strong interaction regimes respectively. First, the local maximum/minimum in $D(s)$ is actually connected to U_{S1} and U_{S2} (both corresponding to $(\partial S/\partial U)_T = 0$) in Fig. 1: the equality $(\partial D/\partial s)_U = (\partial D/\partial T)_U \times [(\partial s/\partial T)_U]^{-1}$ and the Maxwell’s relation $-(\partial D/\partial T)_U = (\partial S/\partial U)_T$ explicitly state that $(\partial D/\partial s)_U = 0$ and $(\partial S/\partial U)_T = 0$ coincide in T - U plane. The U_{S1} curve crosses the vertical $U/t = 6$ line for twice (the cross at $T/t > 0.7$ is not shown), in correspondence to the local minimum (at $s/k_B \simeq 0.72$) and maximum (at $s/k_B \simeq 0.40$) of $D(s)$ for $U/t = 6$ in Fig. 4. Physically, these local extremums signify the crossovers from Bad metal state to Fermi liquid regime and the reverse [34]. In contrast, the situation for $U/t = 10$ is quite different. The local minimum at $s_{\text{min}}/k_B \simeq 0.61$ in $D(s)$

corresponds to U_{S2} , and s_{\min}/k_B should gradually approach the universal number $\ln 2$ as $U/t \rightarrow \infty$ [39]. For this case, the local minimum identifies the spin physics dominated region ($s < s_{\min}$) in the system, which can be effectively described by AFM Heisenberg model. For the intermediate $U/t = 8$, we observe a plateau within $0.25 < s/k_B < 0.65$ in $D(s)$. The other important feature of the $D(s)$ curves is the linear behavior in a low-entropy region containing Néel transitions, especially for $U/t = 6$ and 10. We have also calculated the critical entropy $s_N/k_B = 0.33(1)$, $0.354(7)$ and $0.33(1)$ for the three interactions, where the $U/t = 10$ result is already quite close to that of 3D AFM Heisenberg model [46]. These properties in $D(s)$ can serve as useful probes in optical lattice experiments to detect the MIC in PM phase, effective Heisenberg physics and the Néel transition simply by the double occupancy. We have also checked the results of S_{AFM}^{zz} versus the entropy [47], and confirmed similar critical scaling behavior $(S_{\text{AFM}}^{zz} - S_0) \propto |s/s_N - 1|^{-\gamma}$ as observed in experiment.

In summary, we have systematically studied the interplay between the thermal entropy, density disorder and AFM properties in half-filled 3D Hubbard model following the manner of the most recent optical lattice experiment [25]. We have established the full entropy map on T - U plane for the model, based on which we have resolved the discrepancy between the experiment and theory on the peak antiferromagnetism. More specifically, we have found that the *entropy increase* in experimental measurements during increasing interaction and *density disorder* both induce the peak location shifting of AFM structure factor towards stronger interaction. We have also presented predictions for the universal behaviors of double occupancy versus entropy to probe various properties of the system, which can serve as useful guidance for future experimental studies. Our work have bridged the gap between the most recent experiment and the cutting-edge quantum many-body computations, and have built a paradigm for the benchmark between them, by taking the entropy as a central role and including the density disorder as a realistic issue. This paradigm is important and applicable to the benchmark studies on many other exotic properties of various versions of Hubbard model [9, 10] between experiment and theory.

We thank Xing-Can Yao for valuable discussions on the experimental details. This work was supported by the National Natural Science Foundation of China (under Grants No. 12047502, No. 12204377, and No. 12275263), the Innovation Program for Quantum Science and Technology (under Grant No. 2021ZD0301900), the Natural Science Foundation of Fujian province of China (under Grant No. 2023J02032), and the Youth Innovation Team of Shaanxi Universities.

* yjdeng@ustc.edu.cn

† heyuanhao@nwu.edu.cn

- [1] M. Lewenstein, A. Sanpera, V. Ahufinger, B. Damski, A. Sen(De), and U. Sen, Ultracold atomic gases in optical lattices: mimicking condensed matter physics and beyond, *Advances in Physics* **56**, 243 (2007).
- [2] I. Bloch, J. Dalibard, and W. Zwerger, Many-body physics with ultracold gases, *Rev. Mod. Phys.* **80**, 885 (2008).
- [3] J. Hubbard and B. H. Flowers, Electron correlations in narrow energy bands, *Proc. R. Soc. Lond. Ser. A* **276**, 238 (1963).
- [4] J. Kanamori, Electron correlation and ferromagnetism of transition metals, *Prog. Theor. Phys* **30**, 275 (1963).
- [5] M. C. Gutzwiller, Effect of correlation on the ferromagnetism of transition metals, *Phys. Rev. Lett.* **10**, 159 (1963).
- [6] T. Esslinger, Fermi-hubbard physics with atoms in an optical lattice, *Annual Review of Condensed Matter Physics* **1**, 129 (2010).
- [7] C. Gross and I. Bloch, Quantum simulations with ultracold atoms in optical lattices, *Science* **357**, 995 (2017).
- [8] F. Schäfer, T. Fukuhara, S. Sugawa, Y. Takasu, and Y. Takahashi, Tools for quantum simulation with ultracold atoms in optical lattices, *Nature Reviews Physics* **2**, 411 (2020).
- [9] D. P. Arovas, E. Berg, S. A. Kivelson, and S. Raghu, The hubbard model, *Annual Review of Condensed Matter Physics* **13**, 239 (2022).
- [10] M. Qin, T. Schäfer, S. Andergassen, P. Corboz, and E. Gull, The hubbard model: A computational perspective, *Annual Review of Condensed Matter Physics* **13**, 275 (2022).
- [11] J. P. F. LeBlanc, A. E. Antipov, F. Becca, I. W. Bulik, G. K.-L. Chan, C.-M. Chung, Y. Deng, M. Ferrero, T. M. Henderson, C. A. Jiménez-Hoyos, E. Kozik, X.-W. Liu, A. J. Millis, N. V. Prokof'ev, M. Qin, G. E. Scuseria, H. Shi, B. V. Svistunov, L. F. Tocchio, I. S. Tupitsyn, S. R. White, S. Zhang, B.-X. Zheng, Z. Zhu, and E. Gull (Simons Collaboration on the Many-Electron Problem), Solutions of the two-dimensional hubbard model: Benchmarks and results from a wide range of numerical algorithms, *Phys. Rev. X* **5**, 041041 (2015).
- [12] B.-X. Zheng, C.-M. Chung, P. Corboz, G. Ehlers, M.-P. Qin, R. M. Noack, H. Shi, S. R. White, S. Zhang, and G. K.-L. Chan, Stripe order in the underdoped region of the two-dimensional hubbard model, *Science* **358**, 1155 (2017).
- [13] B. Xiao, Y.-Y. He, A. Georges, and S. Zhang, Temperature dependence of spin and charge orders in the doped two-dimensional hubbard model, *Phys. Rev. X* **13**, 011007 (2023).
- [14] A. Sewer, X. Zotos, and H. Beck, Quantum monte carlo study of the three-dimensional attractive hubbard model, *Phys. Rev. B* **66**, 140504 (2002).
- [15] T. Paiva, R. Scalettar, M. Randeria, and N. Trivedi, Fermions in 2d optical lattices: Temperature and entropy scales for observing antiferromagnetism and superfluidity, *Phys. Rev. Lett.* **104**, 066406 (2010).
- [16] R. A. Fontenele, N. C. Costa, R. R. dos Santos, and T. Paiva, Two-dimensional attractive hubbard model and

- the bcs-bec crossover, *Phys. Rev. B* **105**, 184502 (2022).
- [17] M. Qin, C.-M. Chung, H. Shi, E. Vitali, C. Hubig, U. Schollwöck, S. R. White, and S. Zhang (Simons Collaboration on the Many-Electron Problem), Absence of superconductivity in the pure two-dimensional hubbard model, *Phys. Rev. X* **10**, 031016 (2020).
- [18] H. Xu, C.-M. Chung, M. Qin, U. Schollwöck, S. R. White, and S. Zhang, Coexistence of superconductivity with partially filled stripes in the hubbard model, *Science* **384**, eadh7691 (2024).
- [19] M. Boll, T. A. Hilker, G. Salomon, A. Omran, J. Nespolo, L. Pollet, I. Bloch, and C. Gross, Spin- and density-resolved microscopy of antiferromagnetic correlations in fermi-hubbard chains, *Science* **353**, 1257 (2016).
- [20] L. W. Cheuk, M. A. Nichols, K. R. Lawrence, M. Okan, H. Zhang, E. Khatami, N. Trivedi, T. Paiva, M. Rigol, and M. W. Zwierlein, Observation of spatial charge and spin correlations in the 2d fermi-hubbard model, *Science* **353**, 1260 (2016).
- [21] A. Mazurenko, C. S. Chiu, G. Ji, M. F. Parsons, M. Kanász-Nagy, R. Schmidt, F. Grusdt, E. Demler, D. Greif, and M. Greiner, A cold-atom fermi-hubbard antiferromagnet, *Nature* **545**, 462 (2017).
- [22] E. Cocchi, L. A. Miller, J. H. Drewes, C. F. Chan, D. Perrot, F. Brennecke, and M. Köhl, Measuring entropy and short-range correlations in the two-dimensional hubbard model, *Phys. Rev. X* **7**, 031025 (2017).
- [23] M. Xu, L. H. Kendrick, A. Kale, Y. Gang, G. Ji, R. T. Scalettar, M. Lebrat, and M. Greiner, Frustration- and doping-induced magnetism in a fermi-hubbard simulator, *Nature* **620**, 971 (2023).
- [24] R. A. Hart, P. M. Duarte, T.-L. Yang, X. Liu, T. Paiva, E. Khatami, R. T. Scalettar, N. Trivedi, D. A. Huse, and R. G. Hulet, Observation of antiferromagnetic correlations in the hubbard model with ultracold atoms, *Nature* **519**, 211 (2015).
- [25] H.-J. Shao, Y.-X. Wang, D.-Z. Zhu, Y.-S. Zhu, H.-N. Sun, S.-Y. Chen, C. Zhang, Z.-J. Fan, Y. Deng, X.-C. Yao, Y.-A. Chen, and J.-W. Pan, Antiferromagnetic phase transition in a 3d fermionic hubbard model, *Nature* **632**, 267 (2024).
- [26] L. Niaz and A. Krasnok, Quantum leap: observing antiferromagnetic transition in a 3D fermionic hubbard model with ultracold atoms, *Advanced Photonics* **6**, 060503 (2024).
- [27] J. L. Miller, A quintessential quantum simulator takes a 10 000-fold leap, *Physics Today* **77**, 12 (2024).
- [28] M. Campostrini, M. Hasenbusch, A. Pelissetto, P. Rossi, and E. Vicari, Critical exponents and equation of state of the three-dimensional heisenberg universality class, *Phys. Rev. B* **65**, 144520 (2002).
- [29] R. Staudt, M. Dzierzawa, and A. Muramatsu, Phase diagram of the three-dimensional hubbard model at half filling, *The European Physical Journal B* **17**, 411 (2000).
- [30] T. Paiva, Y. L. Loh, M. Randeria, R. T. Scalettar, and N. Trivedi, Fermions in 3d optical lattices: Cooling protocol to obtain antiferromagnetism, *Phys. Rev. Lett.* **107**, 086401 (2011).
- [31] T. Paiva, E. Khatami, S. Yang, V. Rousseau, M. Jarrell, J. Moreno, R. G. Hulet, and R. T. Scalettar, Cooling atomic gases with disorder, *Phys. Rev. Lett.* **115**, 240402 (2015).
- [32] E. Ibarra-García-Padilla, R. Mukherjee, R. G. Hulet, K. R. A. Hazzard, T. Paiva, and R. T. Scalettar, Thermodynamics and magnetism in the two-dimensional to three-dimensional crossover of the hubbard model, *Phys. Rev. A* **102**, 033340 (2020).
- [33] F. Sun and X. Y. Xu, Boosting determinant quantum monte carlo with submatrix updates: Unveiling the phase diagram of the 3d hubbard model, *arXiv: 2404.09989* (2024).
- [34] Y.-F. Song, Y. Deng, and Y.-Y. He, Extended metal-insulator crossover with strong antiferromagnetic spin correlation in half-filled 3d hubbard model, *arXiv: 2404.08745* (2024).
- [35] Y.-F. Song, Y. Deng, and Y.-Y. He, Magnetic, thermodynamic and dynamical properties of the three-dimensional fermionic hubbard model: a comprehensive monte carlo study, *arXiv: 2407.08603* (2024).
- [36] E. Khatami, Three-dimensional hubbard model in the thermodynamic limit, *Phys. Rev. B* **94**, 125114 (2016).
- [37] F. Werner, O. Parcollet, A. Georges, and S. R. Hassan, Interaction-induced adiabatic cooling and antiferromagnetism of cold fermions in optical lattices, *Phys. Rev. Lett.* **95**, 056401 (2005).
- [38] A.-M. Daré, L. Raymond, G. Albinet, and A.-M. S. Tremblay, Interaction-induced adiabatic cooling for antiferromagnetism in optical lattices, *Phys. Rev. B* **76**, 064402 (2007).
- [39] E. V. Gorelik, D. Rost, T. Paiva, R. Scalettar, A. Klümper, and N. Blümer, Universal probes for antiferromagnetic correlations and entropy in cold fermions on optical lattices, *Phys. Rev. A* **85**, 061602 (2012).
- [40] J. Imriška, M. Iazzi, L. Wang, E. Gull, D. Greif, T. Uehlinger, G. Jotzu, L. Tarruell, T. Esslinger, and M. Troyer, Thermodynamics and magnetic properties of the anisotropic 3d hubbard model, *Phys. Rev. Lett.* **112**, 115301 (2014).
- [41] L. Rampon, F. Šimkovic, and M. Ferrero, Magnetic phase diagram of the three-dimensional doped hubbard model, *arXiv: 2409.08848* (2024).
- [42] E. Kozik, E. Burovski, V. W. Scarola, and M. Troyer, Néel temperature and thermodynamics of the half-filled three-dimensional hubbard model by diagrammatic determinant monte carlo, *Phys. Rev. B* **87**, 205102 (2013).
- [43] C. Lenihan, A. J. Kim, F. Šimkovic, and E. Kozik, Evaluating second-order phase transitions with diagrammatic monte carlo: Néel transition in the doped three-dimensional hubbard model, *Phys. Rev. Lett.* **129**, 107202 (2022).
- [44] R. Garioud, F. Šimkovic, R. Rossi, G. Spada, T. Schäfer, F. Werner, and M. Ferrero, Symmetry-broken perturbation theory to large orders in antiferromagnetic phases, *Phys. Rev. Lett.* **132**, 246505 (2024).
- [45] G. Li, A. E. Antipov, A. N. Rubtsov, S. Kirchner, and W. Hanke, Competing phases of the hubbard model on a triangular lattice: Insights from the entropy, *Phys. Rev. B* **89**, 161118 (2014).
- [46] S. Wessel, Critical entropy of quantum heisenberg magnets on simple-cubic lattices, *Phys. Rev. B* **81**, 052405 (2010).
- [47] See Supplemental Material at <http://link.aps.org/supplemental/xxx> for supplemental results of the full maps for AFM structure factor and double occupancy, and the critical scaling of AFM structure factor versus the entropy.
- [48] Private communication with Xing-Can Yao.

Supplementary material for “Thermal Entropy, Density Disorder and Antiferromagnetism of Repulsive Fermions in 3D Optical Lattice”

THE HEAT MAPS OF AFM STRUCTURE FACTOR AND DOUBLE OCCUPANCY

In Fig. 5, we present the numerical results of the full maps of antiferromagnetic (AFM) structure factor S_{AFM}^{zz} and double occupancy D on T - U plane for 3D half-filled Hubbard model. As expected, the finite-size S_{AFM}^{zz} result is much bigger inside the AFM ordered phase. Note that S_{AFM}^{zz} should diverge in AFM phase and gradually saturate to finite values in paramagnetic (PM) phase as approaching $L = \infty$. The contour lines of double occupancy reveal that this quantity has very weak temperature dependence, especially in PM phase. Moreover, the shape of contour lines of D bends a little bit when crossing the Néel transitions.

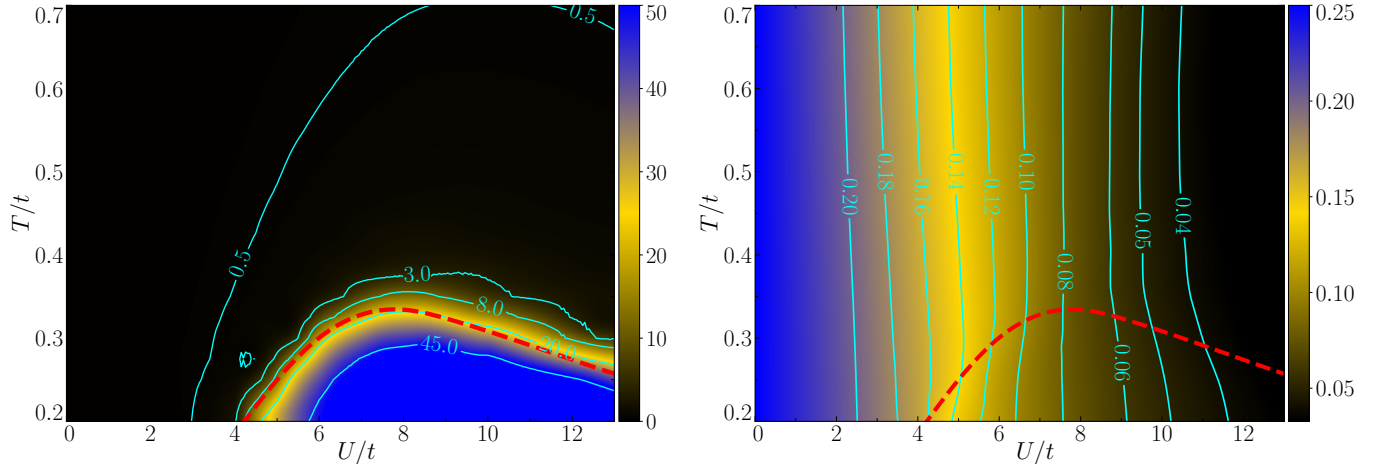


FIG. 5. The heat map of AFM structure factor S_{AFM}^{zz} and double occupancy D on T - U plane for 3D half-filled Hubbard model from our AFQMC simulations. For S_{AFM}^{zz} , the results consist of $L = 12$ data for $T \leq 0.35$ and converged results (to thermodynamic limit) for $T \geq 0.40$. For D , the residual finite-size effect is negligible. The red dashed line plots the Néel temperatures T_N .

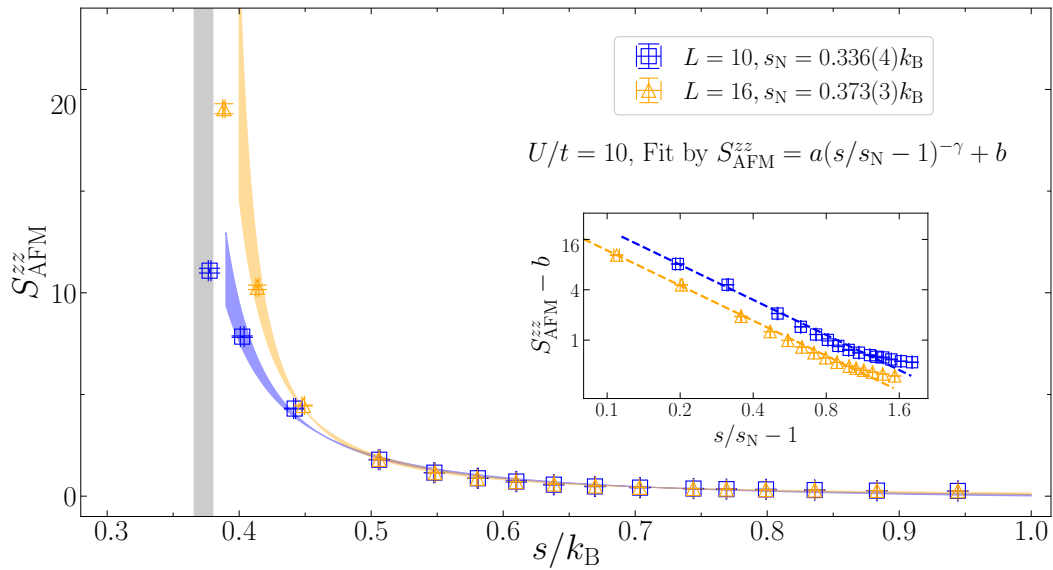


FIG. 6. Critical scaling of S_{AFM}^{zz} versus the entropy per particle s/k_B for $U/t = 10$ with $L = 10$ and $L = 16$, using the relation $S_{\text{AFM}}^{zz} = a(s/s_N - 1)^{-\gamma} + b$ with $\gamma = 1.396$ as the critical exponent from the Heisenberg universality class [28]. The inset is the semi-log plot of $(S_{\text{AFM}}^{zz} - b)$ versus $(s/s_N - 1)$, with dashed lines denoting the fitting curves.

THE CRITICAL SCALING OF AFM STRUCTURE FACTOR VERSUS ENTROPY

In Fig. 6, we present the critical scaling of AFM structure factor S_{AFM}^{zz} versus the thermal entropy per particle s for $U/t = 10$ with $L = 10$ and $L = 16$ systems. We adopt the formula $S_{\text{AFM}}^{zz} = a(s/s_N - 1)^{-\gamma} + b$ for the fitting using the numerical data in PM phase, following the manner in the experiment [25]. The results indeed fits the scaling relation quite well, and the critical extropy s_N/k_B from the fitting is comparable to numbers presented in the main text. We also note that the critical extropy extracted from the experimental data [25] is significantly smaller than our numerical results, such as $s_N/k_B = 0.27(1)$ for $U/t = 11.75$ in experiment comparing to $s_N/k_B = 0.33(1)$ for $U/t = 10$ in our numerics. This disagreement might be attributed to two reasons. First, the experiment data process used the initial single-particle entropy (before loading the optical lattice and adding the interaction), and the experimental measurements with increasing U should have entropy increase as discussed in the main text. Second, the existence of lattice density disorder in the experimental setup should also suppress the Néel transition temperatures of the system, which consequently reduces the critical entropy.